Spectrochimica Acta Part A: Molecular and Biomolecular Spectroscopy 288 (2023) 122148

Contents lists available at ScienceDirect

Spectrochimica Acta Part A: Molecular and Biomolecular Spectroscopy

journal homepage: www.journals.elsevier.com/spectrochimica-acta-part-a-molecular-and-biomolecular-spectroscopy

Spectroscopic evidence of the radioresistance of *Chroococcidiopsis* biosignatures: A combined Raman, FT-IR and THz-TDs spectroscopy study

Elisa Fardelli [a,*], Annalisa D'Arco [b], Stefano Lupi [b,c], Daniela Billi [d], Ralf Moeller [e], Mariangela Cestelli Guidi [c]

[a] University of Roma Tre, Department of Science, Viale G. Marconi, 446, Rome, 00146, Italy
[b] University of La Sapienza, Department of Physics, P.le A. Moro, 5, Rome, 00185, Italy
[c] INFN - LNF, Via E. Fermi, 54, Frascati, 00044, Italy
[d] University of Tor Vergata, Department of Biology, Via della ricerca scientifica, 1, Rome, 00133, Italy
[e] Institute of Aerospace Medicine, section Aerospace Microbiology, Linder Hohe, Cologne, 51147, Germany

HIGHLIGHTS

- *Chroococcidiopsis* radioresistant extremophile cyanobacterium used in space experiments.
- Recognition of biosignatures with Raman, FT-IR and THz-TDs.
- Application of THz-TDs as biomolecular and pathogen detector.

GRAPHICAL ABSTRACT

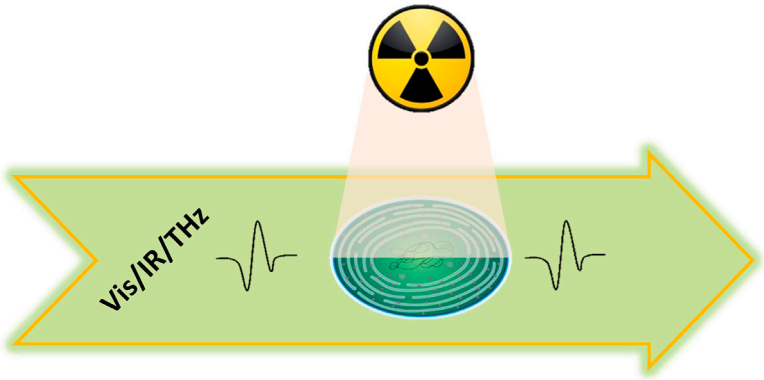

ARTICLE INFO

Keywords:
Raman
FT-IR
THz-TDs
Spectroscopy

ABSTRACT

In the last decades, Mars has been widely studied with on-site missions and observations, showing a planet that could have hosted life in the past. For this reason, the recent and future space missions on the red planet will search for traces of past and, possibly, present life. As a basis for these missions, Space Agencies, such as the European Space Agency, have conducted many experiments on living organisms, studying their behavior in extraterrestrial conditions, learning to recognize their biosignatures with techniques remotely controllable such as Raman spectroscopy. Among these organisms, the radioresistant cyanobacterium Chroococcidiopsis was irradiated during the STARLIFE campaign with strong radiative insults. In this article we have investigated this cyanobacterium using Raman spectroscopy and extended the characterization of its biosignatures and its response to the radiative stress to the mid- Infrared and Terahertz spectral region using the Fourier Transform InfraRed (FT-IR) and Terahertz Time Domain spectroscopy (THz- TDs), which demonstrates the compatibility and suitability of these techniques for future space missions.

* Corresponding author.
E-mail address: fardellielisa91@gmail.com (E. Fardelli).

https://doi.org/10.1016/j.saa.2022.122148
Received 12 July 2022; Received in revised form 7 October 2022; Accepted 11 October 2022
Available online 23 November 2022

1. Introduction

The potential presence of life in our solar and/or in extra-solar systems has always fascinated humanity. With the advent of the space age, interest in the pursuit of life is rapidly increasing, focusing on where and how to recognize life in outer space. Indeed, space explorations and growing knowledge of life on Earth has highlighted potential extraterrestrial targets, which may have harbored life or could maintain hospitable conditions for life, [1,2]. Among these, in the last 20 years, Mars has been the focus of extensive studies and observations by dedicated robotic missions, aimed at acquiring more information about its surface environment. In addition to this, Space Agencies have supported various ground-based and in-space experiments on living organisms, in order to test and study their behavior in extraterrestrial conditions, identify the biosignatures and experimental techniques that would reveal their presence in foreign environments, from those in space to those present on other planets and moons. Extremophile organisms were chosen as potential candidates due to their ability to survive and withstand highly inhospitable conditions, [3–5]. Among these organisms, *Chroococcidiopsis*, a desertic cyanobacterium, exhibits a strong radio-resistance, tolerating high doses of ionizing radiation (i.e. up to 15 kGy at a 100 Gy/min dose rate of γ-rays) [6], high resistance to dry storage up to 4 years, and extreme conditions such as temperature, pressure and vacuum: it survived 548 day is space-like conditions. The radio-resistance of *Chroococcidiopsis* was put to test during the STARLIFE irradiation campaign in 2014, [7]. Two strains of cyanobacteria, *Chroococcidiopsis* CCMEE 029 and *057* dried and in liquid culture, were irradiated with photons (X- and γ- rays) and ions (He, Fe and Si) to compare the different radio responses of both system conditions [6,8]. In this article, we explore the potential of vibrational spectroscopies in ground-based experiments, miming extraterrestrial environmental conditions. We have characterized spectroscopically dried *Chroococcidiopsis* (CCMEE 057) exposed to increasing doses of X-rays during the STARLIFE Irradiation Campaign. In addition to the well-assessed Raman spectroscopy, we enlarged the spectral characterization with Fourier Transform Infrared (FT-IR) spectroscopy and gave a novel insight deep into the IR spectral region using Terahertz Time Domain spectroscopy (THz-TDs). THz spectroscopy enables the detection of bacterial cells based on specific spectral features in the unexplored THz fingerprint, completing their knowledge of the spectral data obtained with IR and Raman spectroscopy, [9,10]. Recently, Yoon et al. 2020 [11] performed measurements of microbial films of various microorganism species: it was found that they have significant differences in their dielectric constants between the types of microorganisms. This reveals the potential of THz spectroscopy in wide applications as biomolecular and pathogens investigations, including the detection of viruses and bacteria, [12–14].

The three techniques are all label free, non-destructive and remotely controllable and, most important, they provide complementary information on the biochemical composition of organisms and on the related modifications induced by radiation [13,15,16]. The goal of this paper is a complete characterization of the spectral biosignatures in the IR range, using different highly sensitive and non-invasive vibrational techniques, which allows to observe any precursor effect of the damage from high doses at the submolecular and collective level; at the same time we want to evaluate potential radio-induced damages and/or alterations of the optical response, compare them in terms of sensitivity and efficacy.

2. Materials and methods

2.1. Preparation of chroococcidiopsis sample

Chroococcidiopsis (CCMEE 057) was chosen as biological model system. Roseli Ocampo-Friedmann isolated *Chroococcidiopsis* from chasmoendolithic growth in granite in the Sinai Desert (Egypt) and it is maintained at the University of Rome Tor Vergata. The strain was grown under routine conditions at 25 °C, in BG11 medium, under a photon flux density of 40 $\mu mol \cdot m^{-2} \cdot s^{-1}$ provided by fluorescent cool-white bulbs with a 16/8 h light/dark cycle.

Chroococcidiopsis (CCMEE 057) was irradiated with increasing doses of ionizing radiations, namely X-ray, with low Linear Energy Transfer during the STARLIFE irradiation campaign in 2014, [7]. CCMEE 057 was therefore kept at the University of Rome Tor Vergata in a sealed eppendorf for 4 years.

Samples used for Raman and FT-IR experiments consist of 10 μl of solution ($\sim 1.5 \cdot 10^9$ cfu/ml) dropped in triplicate on a Si plate and dried in air.

For THz-TDs experiments, a volume of 40 μl of the concentrated solution ($\sim 6.9 \cdot 10^9$ cfu/ml)was deposited on a multiwell Si plate. Details of the sample's preparation can be found in Supplementary Information, SI.

2.2. Raman spectroscopy: experimental set-up and data collection parameters

Raman measurements were performed with a Jasco NRS 5100 micro-Raman in backscattering geometry. A green laser (@ 532 nm) probed the samples using a laser power of 1.3 mW for 5 accumulation of 5 s of exposure each, passing through a confocal microscope (20X objective, which gave a 5 μm-wide laser spot) coupled with a Czerny–Turner spectrometer (1800 gr/mm grating) and a Charged Coupled Device, CCD, as detector (1024 × 256 pixels whose dimension is 26 × 26 μm). Raman spectra range from 800 to 1700 cm^{-1} with a spectral resolution of 4 cm^{-1}.

OPUS 7.0 and Origin 9.0 were used to treat, respectively, the raw Raman spectra and related data in a manner consistent with the method described in [8,17]. After linearly baseline the Raman spectra, the Signal-to-Noise Ratio (SNR) was calculated by dividing the Intensity of the peak at 1516 cm^{-1} (the signal) by the standard deviation of the spectral range 700–900 cm^{-1} (the noise). Spectra whose SNR > 70% were averaged and the resulting spectrum was fitted with Lorentz curves. The intensities of the relative peaks were then normalized to the corresponding bands of the non-irradiated sample (the control), expressing the intensities in normalized values.

2.3. FT-ir spectroscopy: experimental set-up and data collection parameters

FT-IR spectroscopy of a biological material is a direct method to extract biochemical information in a non destructive and label-free way [18]. Molecular bonds with a variable electric dipole moment due to vibrations are IR active. It is a very versatile technique and over time it has proven to be a strategic tool in several research fields; for example, to monitor the radiation-induced damage of biomolecules such as DNA, proteins and lipids. More in detail, ionizing radiation damages molecular structures and it is possible to record its effect based on the modification of the FT-IR spectral characteristics of the biomolecules [19–24]. Furthermore, FT-IR and Raman spectroscopies are often coupled together to characterize the molecular composition of the sample in a complementary way, since in parity of conserved materials Raman active rotovibrations are not FT-IR active and vice versa [16,25].

FT-IR measurements were performed in transmission geometry with an IR microscope (Bruker Hyperion 3000). In detail, the experimental set-up consists of a mid-IR source (globar), illuminating a Michelson interferometer (Bruker, Vertex 70V) which is coupled with the IR microscope (equipped with Cassegrain objectives, and a magnification of 15X) and an IR detector, a 0.25 × 0.25 mm Mercury Cadmium Telluride (MCT). The FT-IR measurements absorbance spectra averaged 64 scans over a 700–3800 cm^{-1} spectral range with spectral resolution of 4 cm^{-1}.

OPUS 7.0 and Origin 9.0 were employed to treat, respectively, the FT-IR raw spectra and related data, respectively. The FT-IR spectra were vector normalized and baseline corrected using the OPUS software functions. Once the bands of interest were identified, they were deconvoluted with Lorentz curves to reveal the underlying peaks and their characteristics.

2.4. THz-TDs spectroscopy: experimental set-up and data collection parameters

THz spectral range (3–300 cm^{-1}, or 0.1 to 10 THz) has quickly become accessible thanks to many efforts made in THz technology and in the improvement of THz sources and detectors, [26–32], stimulating an extensive and rapid spread of THz radiation in various scientific fields, [29,33–40]. THz photons (equivalent to 4meV @ 1 THz) propagate through biological targets in order to excite collective low-frequency vibrational modes, i.e coinciding with the energy levels related to rotational and vibrational molecular modes and intermolecular vibrations, such as hydrogen bonds, van der Waals forces and non-bonding (hydrophobic) interactions, [41]. Furthermore, the THz sensitivity to polar molecules, including water molecule [42,43], makes it possible to quickly assess the life status of bacteria by evaluating their different level of hydration from a label-free measurement. In particular, differently from IR spectroscopy, THz-TDs employs the synchronous and coherent detection of THz electric field both in amplitude and phase, allowing the evaluation of the optical parameters of the sample without using Kramer–Kronig equations. THz electric fields of irradiated dried CCMEE057 were collected with the home-made THz-TDs spectrometer (reported in THz-TDs Section of SI). The system works in transmission mode and in the spectral range between 0.2–2.5 THz. The empty Si plate (reference signal) and sample pulses are measured by placing the Si plate with dried cyanobacteria in the focal point of THz radiation, respectively, with an approximately 1 mm spot diameter under ambient conditions, [33]. Each measured data point in each sample was averaged ten times in the time domain, and all measured data were averaged five times. Time-domain data were converted into frequency-domain data using a fast Fourier transform (FFT) algorithm in Matlab2016b. By measuring both the amplitudes and phases of the transmitted THz pulses through the thick bacterial depositions, we extracted the complex dielectric constants (see SI).

3. Results

3.1. Raman spectroscopy results

In order to study the effects of radiation on *Chroococcidiopsis*, a Raman study was performed by measuring the spectra related to CCMEE 057 irradiated with each dose (see Sample Treatment section in SI). The preliminary study of the wide range (300–5500 cm^{-1}) spectra showed the fingerprint of the carotenoids at low frequencies (from 900 to 1600 cm^{-1}) and a strong fluorescence tail at higher frequencies (shown Figure S1 of SI). Therefore, the following measurements and analyses focused on the carotenoid fingerprint (Fig. 1).

Carotenoids are a variated chemical group having a polyene skeletal backbone, whose Raman spectrum of carotenoids presents three main bands: the C=CH_3 bending (ν_1), the CC stretching (ν_2) and the C=C stretching band (ν_3) [17,44–46]. Furthermore, such Raman spectrum is so stronger to cover the signal coming with respect to other electronic bands because of the Raman Resonance effect. It consist of an increase of the Raman signal of a given electronic band due to the proximity of its energy level and the frequency of the excitation laser [44,46].

The X-ray irradiation that CCMEE 057 experienced did not deteriorate the carotenoid Raman signal also at the highest doses (see Fig. 1). Indeed, the carotenoids Raman spectra are always well recognizable. Moreover, there were no alterations of the three bands parameters in relation to increasing doses. The average frequencies of the bands are the following: ν_1 = 999.8 ± 4 cm^{-1}, ν_2 = 1153.1 ± 4 cm^{-1}, ν_3 = 1514.7 ± 4 cm^{-1} with a variance from the mean values of ca. 0.1. The intensities of the main carotenoid bands showed similar results: as shown in Fig. 2, where the normalized intensity of the three bands is constant at ~ 100%. Indeed, the normalized intensity of the three bands was linearly fitted and for all the datasets the intercept is close to 100% and the slope is ~0 with a mean R^2 ~0.3 (Table 1). These results demonstrate that the intensity of ν_1, ν_2 and ν_3 bands does not vary with increased X-ray doses and, thus, it is not possible to highlight any Raman-spectral modification induced by the radiative insult.

Table 1
Parameters of the linear fit of the normalized intensity of the main carotenoids peaks (ν_1, ν_2, ν_3), which correspond to the y, in relation to the X-ray doses (x) in Fig. 2.

	Linear Fit :	$y(x) = y_0 + xq$	
Normalized Intensity	y_0	q	R^2
ν_1	104 ± 2	−1.4 ± 0.8	0.4
ν_2	105 ± 2	−1.3 ± 0.8	0.4
ν_3	100.01 ± 0.01	$-2 \cdot 10^{-3} \pm 5 \cdot 10^{-3}$	0.03

3.2. FT-IR spectroscopy results

In order to enrich the knowledge on the effects of irradiation on CCMEE 057 and the spectroscopic characterization, the system was studied also with FT-IR and THz-TDs spectroscopies.

The FT-IR spectra of control and irradiated samples are reported in Fig. 3. Inspection of these data by eye is limited as the spectra are qualitatively very similar.

Therefore, to observe overall trends in the data and to determine if the response of X-ray irradiated *Chroococcidiopsis* was characterized by changes to specific biomolecules, the ratios of intensities of specific IR regions were plotted against dose. As lipid levels are fundamental to the integrity and functionality of membranes [47–50], lipid FTIR absorption bands have been analyzed in detail to assess if ionizing radiation may have significant implications for the long-term metabolism and functionality, while Verseux et al. 2017 [6] have shown that no significant structural damage affects lipid membranes after exposure of *Chroococcidiopsis CCMEE 029* dried cells to 5 kGy of X-rays.

The lipid stretching band (2800–3000 cm^{-1}) was deconvoluted with five Lorentz curves: ν_{I1}, ν_{I2}, ν_{I3}, ν_{I4} and ν_{I5}, as shown in Figure S2 and Table S1 of SI, which correspond to the symmetric and antisymmetric stretching *CH* modes. The identified modes were the following:

- ν_{I1} → 2853 cm^{-1} - CH_2 symmetric stretching,
- ν_{I2} → 2873 cm^{-1} - CH_3 symmetric stretching,
- ν_{I3} → 2893 cm^{-1} - *CH* stretching,
- ν_{I4} → 2927 cm^{-1} - CH_2 antisymmetric stretching,
- ν_{I5} → 2960 cm^{-1} - CH_3 antisymmetric stretching.

Variations of frequency and the area ratio are conformation-sensitive and indicate the modification of the membrane bonds, [51]. Though, the analysis of the frequency of ν_{I1}, ν_{I2}, ν_{I3}, ν_{I4} and ν_{I5} did not highlight any significant shift correlated to the irradiation stress, as shown in Figure S3 of SI, giving the suggestion that the irradiation did not affect the inner order of the lipid molecular bonds.

To further prove this thesis, changes to the lipid content of cells were quantified by measurement of the peak intensity of the CH_2 asymmetric stretching and *CH* stretching, CH_2 asymmetric stretching and total lipid band, and the CH_2/CH_3 symmetric stretching, which are correlated, respectively, to the polarity, length and packing of the lipid chains of the membrane, [50,52]. Any variation of these ratios points to the impairment of the integrity of membranes due to the radiative assault, [50]. In all the three cases the ratio did not change with increasing X-ray doses: the polarity is stable at ~7, the length at ~0.9 and the packing at ~0.6. as shown in Fig. 4 and Table 2.

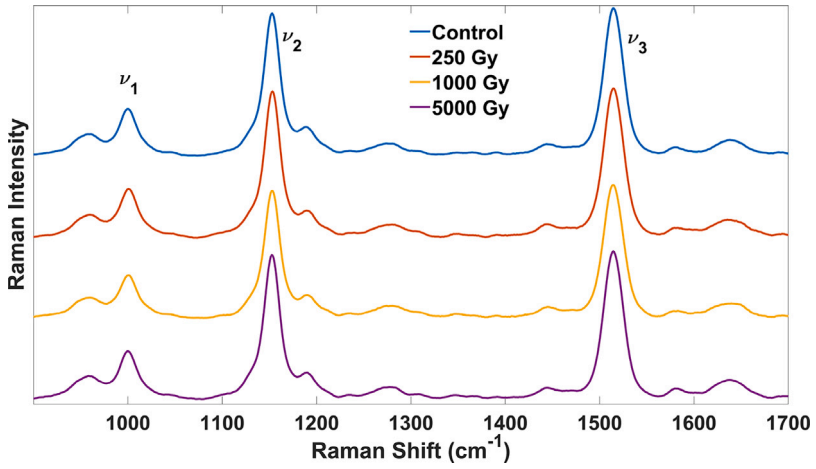

Fig. 1. Representative Raman Spectra of *Chroococcidiopsis* exposed to X-ray irradiation, showing the Raman fingerprint of carotenoids. The spectrum of the control (0 Gy) sample is shown in blue, the sample irradiated with 250 Gy in red, with 1000 Gy in yellow and with 5000 Gy in purple.

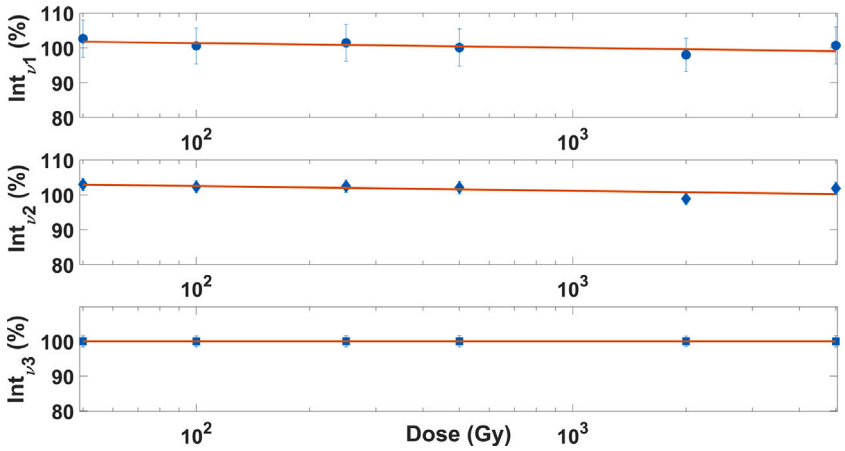

Fig. 2. Normalized intensity of ν_1, ν_2 and ν_3 bands of the X - Ray irradiation series and the relative linear fit (red lines): the intensity of ν_1 band is shown with dot marks, ν_2 with diamonds and ν_3 with squares.

Table 2
Parameters of the linear fit of the normalized intensity of the area ratios of the lipid peaks, which correspond to the y, in relation to the X-ray doses (x) in Fig. 4.

	Linear Fit :	$y(x) = y_0 + xq$	
	y_0	q	R^2
A_{CH2as}/A_{CHs}	7 ± 1	0.25 ± 0.12	0.10
A_{CH2as}/A_{tot}	0.86 ± 0.06	0.014 ± 0.022	0.08
A_{CH2ss}/A_{CH3ss}	0.6 ± 0.1	0.025 ± 0.03	0.12

Also, the protein/lipid ratios were calculated by dividing the intensities of spectral regions associated with proteins (amide and amine regions) by regions associated with lipids (aliphatic *CH* vibration and CH_2/CH_3 asymmetric stretch). As the amount of proteins and lipids play an important role in maintaining function and fluidity, protein/lipid ratios can be related to membrane integrity. These analyses showed that also the protein/lipid ratio remains constant after irradiation (data not shown). It is therefore possible to conclude that an evident change in the metabolic spectral signature of the cells after X-ray irradiation was not evidenced by the FT-IR data.

3.3. THz-TDs spectroscopy results

The previous spectroscopy techniques did not highlight any direct radiation-induced damages at molecular level; thus, the analysis was expanded at collective molecular level through THz-TDs revealing any possible variations induced by secondary effects of radiations such as the reassembly of molecules.

We investigated the dielectric properties of cyanobacterial dried films, previously exposed to increasing X-rays doses. By measuring both amplitudes and phases of the transmitted THz electric fields through the microbial samples, we extracted the dielectric properties, including absorbance and refractive index, representative dielectric constants of the microbial films.

We expect to observe predominantly the spectral contribution due to the bacterial cell wall, as demonstrated by Yoon et al. 2020 [11], in a strong correlation between dielectric constant of cell wall composition and their molecular structures in the study of different types of micro-organisms with THz spectroscopy.

To proceed with this analysis, the samples had to be characterized in this spectral region and Fig. 5 shows the first THz absorption spectra of CCMEE 057 varying the X-rays doses, in the spectral range 0.5–2.5 THz. In Table S2 of SI and in Fig. 6, the position of peaks for samples of control (0 Gy) and exposed to different doses are reported. All the resolved peaks are shown in Fig. 5. In addition, 2nd-derivative analysis of the spectra (data not shown) of control allowed the identification of other contributions, [13,53–56].

The cell wall of cyanobacteria, being Gram-negative bacteria, appears multilayered and the chemical constituents are polypeptide units (called peptidoglycans), which are generally made up of N-acetylmuramic acid (NAM) and N-acetyl-glucosamine (NAG) sugar units, and

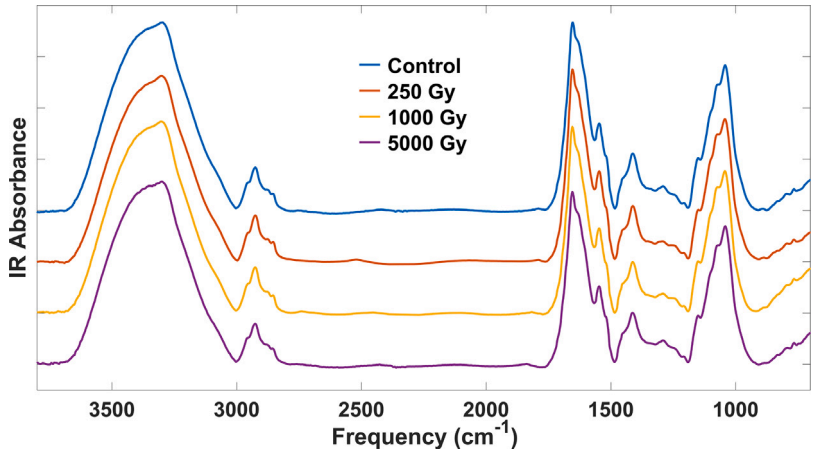

Fig. 3. Representative FT-IR absorbance spectra of X-ray irradiated bacteria shifted for clarity: control (0 Gy) is depicted in blue, 250 Gy in red, 1000 Gy in yellow and 5000 Gy in purple.

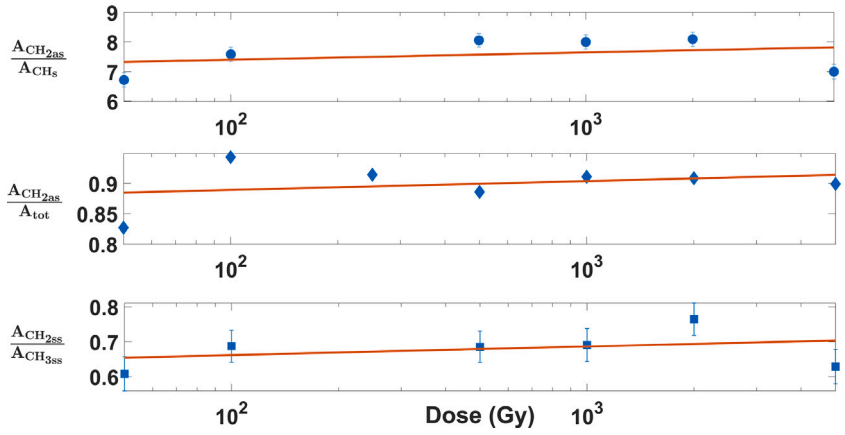

Fig. 4. The top graph shows the area ratio of CH_2 antisymmetric stretching and *CH* stretching (ν_{I4} and ν_{I3}), the middle one of CH_2 antisymmetric stretching (ν_{I4}) and total lipid band and the bottom one of CH_2 and CH_3 symmetric stretching (ν_{I1} and ν_{I2}), which are correlated, respectively, to the polarity, length and packing of the lipid chains of the cyanobacterial membrane. Any variation of these ratios points to the impairment of the integrity of membranes due to the radiative assault. A linear fit was performed on all the datasets (red lines) and in all cases the $R^2 \sim 0.1$ demonstrating that there is no correlation between the ratios and the received doses, the parameters of the linear fits are in Table 2.

peptide chains for crosslinking the repeating chain of sugar molecules, [57].

The THz results, instead, in spectral range from 0.5 to 2.5 THz, are characterized by weak absorption bands below 1 THz, the majority of them can be ascribed to skeleton torsion due to the glycan constituents, Fig. 6. Around 0.9 THz a common absorption feature is observed and attributable to amino acids made up the peptidoglycan unit. Due to the similarity in their chemical structures therefore we cannot assign a unique contribution. A broad absorption band is observed at 1.36 THz attributable to polyglycine, therefore identifying N-Acetyl-D-Glucosamine, [58–60]. Even absorption frequencies around 1.84 and 2.30 THz can be ascribed to L-glycine, [58,61]. In addition, L- and D- glutamic acid exhibit resonant frequencies at 2.48 and 1.21 THz, respectively, present in the cell wall of bacteria, [58,62–64].

We are able to identify the absorption features of the sugar unit clearly observed around 1.76 THz. The intense broad band, centered around 2.14 THz, is the convolution of partially overlapping spectral contributions due to the deformation skeleton of the sugar rings, L-lysine, D- and L-alanine and L-glutamic acid, [58,62,65–68].

The ripples around 1.15 THz and 2.25 THz are observed in the spectra of bacteria exposed to 0 and 500 Gy. They are due to the remnant THz water absorption in the sample not completely dried. Notably, for the spectral region below 1 THz, the band at 0.76 THz, related to glycans, shows shifts beyond the spectral resolution (0.05 THz), toward lower frequencies for 250 Gy, 500 Gy and 1000 Gy. It is worthwhile to note that changes in lipid-related peaks are usually associated with activation of peroxidases and glucose catabolism, [69]. Although, some studies on the effects of ionizing radiations on cyanobacteria have also shown that some of the cyanobacteria can tolerate very high doses as well as chronic low dose of ionizing radiation, chronic exposure could stimulate effects, such as activation of peroxidases and glucose catabolism, and/or indirect effects due to the ROS action, [3,70–72]. In the same frequency region, a significant shift is observed for 0.92 THz peak related to amino acids contribution for biofilm exposed to 1000 Gy dose. The two resolved bands at 1.76 and 1.92 THz, related to the sugar and glycine contributions respectively, shift in order to form a unique broadband with the spectral contents reported in the Table S2 of SI. In conclusion, from the comparison of THz absorption spectra between the control biofilm and those exposed to various X-rays doses emerges that they have similar THz absorption characteristics, originating from the same molecular collective vibration modes. As expected, these reflect the bacterial membrane composition. No relevant radio induced direct effect can be observed.

The representative dielectric constants ϵ_{film} of the CCMEE 057 targets are estimated for the five different X-rays doses, (see SI). The imaginary parts are close to zero. Assuming this as a starting point, the dielectric properties of individual CCMEE 057 could be obtained. We used the effective medium theory, specifically the Bruggeman

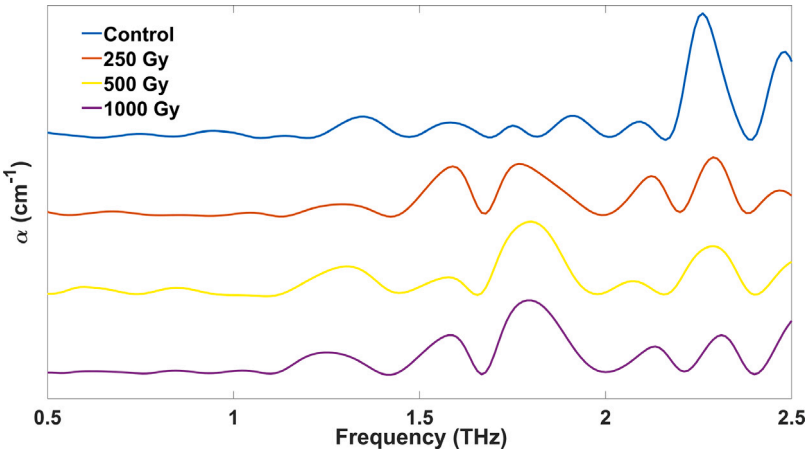

Fig. 5. THz absorption spectra of dried CCMEE 057 films on Si substrate exposed to increasing X-rays doses, during the STARLIFE campaign. The spectral range is 0.5–2.5 THz.

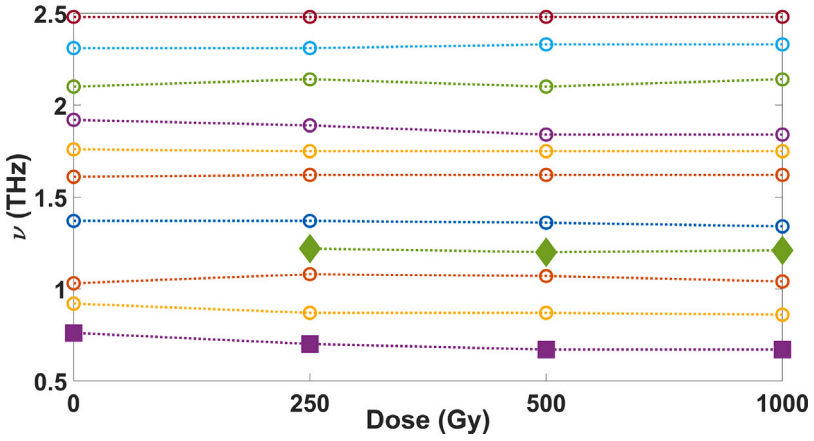

Fig. 6. Frequency shifts of peak positions with respect to those found for the control in the spectral range 0.5–2.5 THz. The shifts whose error is lower than the spectral resolution are reported as circles (with pointed lines for clarity).

model, [73], for which

$$\frac{\epsilon_{\text{film}} - 1}{3\epsilon_{\text{film}}} = \frac{f(\epsilon_{\text{f}} - 1)}{\epsilon_{\text{f}} + 2\epsilon_{\text{film}}} \tag{1}$$

being the imaginary parts close to zero, thus the extinction coefficient is negligible

$$\frac{n_{\text{film}}^2 - 1}{3n_{\text{film}}^2} = \frac{f(n_{\text{f}}^2 - 1)}{n_{\text{f}}^2 + 2n_{\text{film}}^2} \tag{2}$$

Where ϵ_{film} and ϵ_{f} are the real parts of dielectric constants of bacterial film and individual bacteria, respectively; and f is the packing fraction. It strongly depends on the shape of the individual microorganisms volume fraction and aspect ratio because they influence the arrangement in the closely packed films. In order to choose the appropriate value for f, we evaluated the morphological features through an optical microscope. We observed spherical shape (diameter around 2 μm) and high closely packed structure, as displayed in an optical microscope picture of deposited bacterial cells on Si substrate (in SI). Therefore, we assume $f = 0.64$, [11,73,74]. The refractive indices are displayed in Fig. 7.

The results reported here can be considered as a first starting point to evaluate the potentiality of THz spectroscopy in this research field. The extrapolated optical properties of cyanobacteria exposed to increasing doses of X-ray radiations are in accordance with the results achieved to Raman and FT-IR spectroscopies. Moreover, they could be used as biomarkers/biosignatures for the recognition of cyanobacterium CCMEE 057.

Discussion and conclusion

The Raman measurements of this work showed the clear and well recognizable carotenoids biosignature for all the CCMEE 057 samples, also for the one irradiated at the highest dose (5 kGy), Fig. 1. Baqué et al. 2020 identified which genes encode carotenoids for *Chroococcidiopsis* CCMEE 029 and so, which carotenoids are produced: *β*-carotene, hydroxylated carotenoids (zeaxanthin), keto-carotenoids (canthaxanthin and echinone), and of carotenoid glycosides (4-ketomyxol 20-fucoside). Such a great variety of carotenoids guarantee for an efficient ROS scavenging system, [8,44,75,76]. Indeed, the same biosignature was detected when the *Chroococcidiopsis* strain CCMEE 029, was irradiated with γ - rays, doses up to 103 kGy, during the STARLIFE irradiation campaign, [8]. Both strains preserve the spectral characteristics of the carotenoids biosignature regardless of the received dose. Though, there is a slight difference when it comes to comparing the normalized intensity of the main carotenoids peaks: CCMEE 029 intensity decreases by 20% with respect to the control sample while CCMEE 057 is stationary as the X-ray doses increase. This could be explained by the highest dose reached with the γ - rays, though the strength of the carotenoid's biosignature is still remarkable. Moreover, it is worth observing that during the STARLIFE irradiation campaign also the *Nostocales* cyanobacterium was irradiated with γ-rays in dry state or mixed with Mars-like regolith. The following Raman analysis showed that *Nostocales* lost the carotenoids biosignature after it was directly irradiated with more then 12 kGy, demonstrating that the γ-rays damaged the carotenoids molecular structure and that the radioresistance of biosignatures is speci-specific. Though, when *Nostocales*

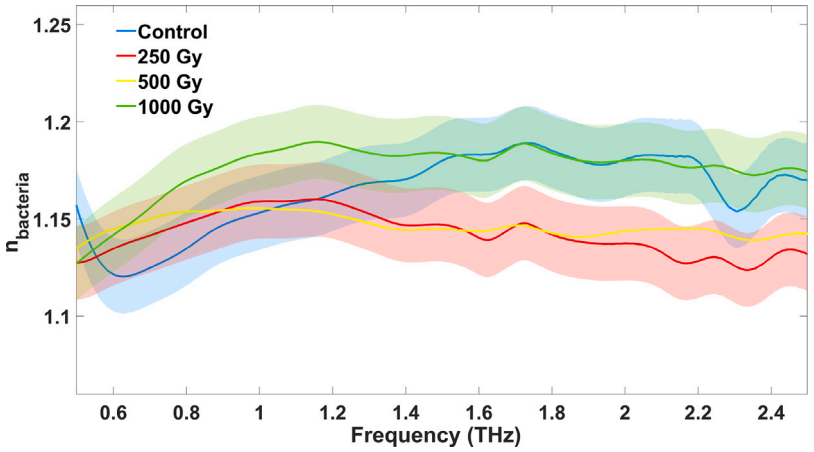

Fig. 7. THz refractive indices of dried CCMEE 057 cyanobacteria obtained from the Bruggeman model exposed to increasing X - rays doses, during the STARLIFE campaign. The spectral range is 0.5–2.5 THz.

was irradiated within Mars-like regolith it successfully endured the radiative-stress and preserved the biosignatures also at the highest dose (over 100 kGy), [17]. Thus, it is possible to conclude that the waterless martian subsoil may preserve the structural integrity of past life and protect the present one, enabling their detection. For all these reasons and for being greatly adaptable Raman spectroscopy has been chosen as the main technology on Perseverance and EXOMARs payload to search for life traces on Mars and due to these characteristics, the carotenoid fingerprint has been chosen as one of the biosignatures that ExoMars and Perseverance will look for on the Red Planet, [6,8,17,77,78].

The FTIR spectra showed five different bands associated with proteins, polysaccharides, water and lipids and none of them displayed any significant modification in correlation to the doses, moreover the spectra were well recognizable despite of the radiative insult. In particular, this study focused on lipids in order to evaluate if there was any variation in the state of the lipid membrane induced by the X-rays. The peaks of the lipid band are conformation-sensitive and variations of frequency and intensity ratios correspond to changes of the membrane status. In particular, the analysis of the frequencies of the lipid peaks did not highlight any shift correlated to the irradiation doses, indicating that there were no variations of the inner order of the lipid membrane. This result was double-proven by the analysis of the membrane's integrity, which did not highlight any variation of the lipid chain polarity, length and packing of the lipids correlated to the X-ray doses, pointing to intact membranes. The absence of physical damages to the bacterial membrane was also observed by Verseux et al. 2017, [6], who demonstrated that irradiated CCMEE 057 with X-rays during the STARLIFE campaign had intact membranes by staining the irradiated cyanobacteria with SYTOX green dye, which penetrates cells with impaired membranes, and even at the highest doses CCMEE 057 was not painted by SYTOX green. Moreover, in the same study the clonogenicity of CCMEE 057 was put to test and it showed that it was still able to replicate after the highest dose of X-ray and after 11 kGy of γ-ray, [6], demonstrating that also the highest doses of X-ray did not structurally damage the membrane or their clonogenicity.

Finally, THz-TDs gave insights on the effect that the X-ray irradiation may have produced at the collective molecular level. THz spectroscopy is largely appealing for biomedical issues, including pathogens detection. In fact, many rotational and vibrational energy levels, and collective modes are located within the THz spectral range providing chemical specificity, which can be efficiently done in label-free and non-contact modes, [12,37]. This may be useful in the characterization of the bacterial cell, spore and intracellular metabolite as distinct spectral signatures in the THz spectra. Differences in THz optical constants enable the differentiation between bacterial species, [10,13,42,79]. Despite this, few work has been done on bacteria in THz spectral region, [10,13,42,79,80].

Here, we reported the first, to our knowledge, THz characterization of optical properties for the cyanobacterium CCMEE 057 exposed to various X-rays doses. As expected, we observed predominantly the spectral contribution due to the bacterial cell wall. The second derivative analysis ensured the identification of characteristic absorption features of bacterial cell constituents: sugar unit, clearly observed around 1.76 and 1.92 THz, and common absorption features attributable to amino acids made up the peptidoglycan units. No significant frequency shifts, that could indicate a potential biomolecula damage induced by ionizing radiation, are observed between the various samples.

All this is reflected in refractive indices. We extrapolated the refractive indices of dried CCMEE 057 cyanobacterium obtained from the Bruggeman model exposed to increasing X-rays doses. Their values are around to 1.15, without significative differences. These results can be considered as a first starting point to evaluate the potentiality in the use of THz spectroscopy for the monitoring of pathogens presence, including bacteria. The extrapolated THz optical properties of cyanobacterial cells exposed to increasing doses of X-ray radiations are in accordance with the results achieved to Raman and FT-IR spectroscopies, which demonstrate that X-rays radiation, also at high doses, did not structurally damaged the membrane, in accordance with the results of Baque et al. 2018 and 2020 Verseux et al. 2017, [6,8,17]. However, other steps are needed before such a technique is established as a predictor of a biological detector, especially in this case where the biological target is continuous exposure at ionizing radiation. In fact, our results pertain strictly to dried cyanobacteria much time after the radiative insult. During this temporal interval, the pathological agents may repair the induced damage, [81]. In fact, it is known that for several hours after irradiation cellular organisms try to repair radiation-induced damage and any damage fraction is eliminated in the sample preparation. Therefore, future measurements should be performed using all exposed populations and at different times after exposure, in order to evaluate the evolution over time and to have similar conditions of space explorations.

It is worth noticing that *Chroococcidiopsis* has an innate resistance towards dehydration, thanks to anhydrobiosis it is able to enter a dormant phase and produce high quantities of compatible solutes, as trehalose and sucrose, which protect the hydration layers around strategic molecules, as proteins, preserving their 3D structure and their functionality, [8,47,82–84]. Indeed, Baque et al. 2020 [8] and Verseux et al. 2017 [6] propose anhydrobiosis as the probable reason for the great resistance of *Chroococcidiopsis* against radiations; indeed, they show that dry CCMEE 057 irradiated with over 100 kGy of γ-rays kept showing highly recognizable carotenoid biosignature even though clonogenicity was totally lost, demonstrating that anhydrobiosis could actively help preserving molecular structures and the relative

biosignature. In addition to this, the lack of water and the high concentration of carotenoids and pigments in CCMEE 057 reduce the formation of Reactive Oxygen Species (ROS), which cause the great majority of radio-induced damages, further, protecting the molecular structure, [76].

These phenomena may be the basis of the great radio-resistance of the biosignatures of CCMEE 057 shown by the three spectroscopic analyses of this study. Indeed, the samples were irradiated in a dry state and kept dry for four years before these spectroscopic analyses and, yet, none of them highlighted any relevant modification of the spectra correlated to the X-ray irradiation, demonstrating that the molecular structure of CCMEE 057 was not damaged by the radiative insult and the dry period, resulting in the preservation of all biosignatures well detectable with Raman, FT-IR and THz-TDs spectroscopy. To conclude, these results demonstrate that FT-IR and THz-TDs are complementary techniques to Raman spectroscopy enlarging the comprehension of the analyzed systems and opening the way for future studies and technological improvements for space missions searching life-traces on other planets and moons.

Funding

SL was founded by NATO Science for Peace and Security Programme under grant No. G5889–"SARS-CoV-2 Multi-Messenger Monitoring for Occupational Health & Safety-SARS 3M" and LazioInnova "Gruppi di Ricerca 2020" of the POR FESR 2014/2020-A0375-2020-36651 project entitled "DEUPAS -DEterminazione Ultrasensibile di agenti PAtogeni mediante Spettroscopia" for the Raman set-up and THz-TDs set-up. MCG by the Dafne Light Lab in the National Laboratories of Frascati for the FT-IR set-up, the samples were prepared and irradiated thanks to ASI BIOSIGN_Cyano 2018-15-U.0 that supported DB and the DLR grant FuE-Projekt "ISS LIFE" (Program RF-FuW, TP 475) RM.

CRediT authorship contribution statement

Elisa Fardelli: Study conception and experimental design, Sample preparation, FT-IR, Raman and THz-TDs data collection and analysis. **Annalisa D'Arco:** Study conception and experimental design, THz-TDs data collection and analysis. **Stefano Lupi:** Study conception and experimental design. **Daniela Billi:** Study conception and experimental design, Sample supply and preparation. **Ralf Moeller:** Study conception, experimental design and sample supply. **Mariangela Cestelli Guidi:** Study conception and experimental design, FT-IR data collection and analysis.

Declaration of competing interest

The authors declare that they have no known competing financial interests or personal relationships that could have appeared to influence the work reported in this paper.

Data availability

Data will be made available on request.

Acknowledgments

The authors thank the Biology department of Biology, the MAECI Graphene3D, Sapienza Terahertz laboratories in the University of Sapienza and the Dafne Light Lab in the National Laboratories of Frascati.

Sample availability

Chroococcidiopsis strains are available upon request from the authors.

Appendix A. Supplementary data

Supplementary material related to this article can be found online at https://doi.org/10.1016/j.saa.2022.122148. In detail, the supplementary material regards the sample preparation, the Raman and FT-IR spectra treatment and the THz-TDs analysis.

References

[1] D.J. Des Marais, J.A. Nuth, L.J. Allamandola, A.P. Boss, r.J.D. Farme, T.M. Hoehler, B.M. Jakosky, V.S. Meadows, A. Pohorille, B. Runnegar, A.M. Spormann, The NASA Astrobiology Roadmap, Astrobiology 8 (4) (2008) 715–739, http://dx.doi.org/10.1089/ast.2008.0819.

[2] G. Horneck, N. Walter, F. Westall, J.L. Grenfell, W.F. Martin, F. Gomez, S. Leuko, N. Lee, S. Onofri, K. Tsiganis, R. Saladino, E. Pilat-Lohinger, E. Palomba, J. Harrison, F. Rull, C. Muller, G. Strazzulla, J.R. Brucato, P. Rettberg, M. Capria, AstRoMap European astrobiology roadmap, Astrobiology 16 (3) (2016) 201–243, http://dx.doi.org/10.1089/ast.2015.1441.

[3] D. Billi, E.I. Friedmann, K.H. Hofer, M. Grilli Caiola, R. Ocampo-Friedmann, Ionizing-Radiation Resistance in the Desiccation-Tolerant Cyanobacterium *Chroococcidiopsis*, Appl. Environ. Microbiol. 66 (4) (2000) 1489–1492, http://dx.doi.org/10.1128/AEM.66.4.1489-1492.2000.

[4] D. Billi, M. Potts, Life and death of dried prokaryotes, Res. Microbiol. 153 (1) (2002) 7–12, http://dx.doi.org/10.1016/s0923-2508(01)01279-7.

[5] M. Baqué, J. de Vera, P. Rettberg, D. Billi, The BOSS and BIOMEX space experiments on the EXPOSE-R2 mission: Endurance of the desert cyanobacterium *Chroococcidiopsis* under simulated space vacuum, Martian atmosphere, UVC radiation and temperature extremes, Acta Astronaut. 91 (2013) 180–186, http://dx.doi.org/10.1016/j.actaastro.2013.05.015.

[6] C. Verseux, M. Baqué, R. Cifariello, C. Fagliarone, M. Raguse, R. Moeller, D. Billi, Evaluation of the Resistance of *Chroococcidiopsis* spp. to Sparsely and Densely Ionizing Irradiation, Astrobiology 17 (2) (2017) 118–125, http://dx.doi.org/10.1089/ast.2015.1450.

[7] R. Moeller, M. Raguse, S. Leuko, T. Berger, C. Hellweg, A. Fujimori, R. Okayasu, G. Horneck, STARLIFE – An international campaign to study the role of galactic cosmic radiation in astrobiological model systems, Astrobiology 17 (2) (2017) 101–109, http://dx.doi.org/10.1089/ast.2016.1571.

[8] M. Baqué, A. Napoli, F. Claudia, R. Moeller, J. de Vera, D. Billi, Carotenoid Raman Signatures are Better Preserved in Dried Cells of the Desert Cyanobacterium *Chroococcidiopsis* than in Hydrated Counterparts after High-Dose Gamma Irradiation, Life 10 (6) (2020) 83–95, http://dx.doi.org/10.3390/life10060083.

[9] C. Wang, J. Gong, Q. Xing, Y. Li, F. Liu, X. Zhao, L. Chai, C. Wang, A.M. Zheltikov, Application of terahertz time-domain spectroscopy in intracellular metabolite detection, J. Biophotonics 3 (10–11) (2010) 641–645, http://dx.doi.org/10.1002/jbio.201000043.

[10] W. Zhang, E.R. Brown, L. Viveros, K.P. Burris, C.N. Stewart, Narrow terahertz attenuation signatures in *Bacillus thuringiensis*, J. Biophotonics 7 (10) (2014) 818–824, http://dx.doi.org/10.1002/jbio.201300042.

[11] S.A. Yoon, S.H. Cha, S.W. Jum, S.J. Park, J.Y. Park, S. Lee, H.S. Kim, Y.H. Ahn, Identifying different types of microorganisms with terahertz spectroscopy, BOE 11 (1) (2020) 406–416, http://dx.doi.org/10.1364/BOE.376584.

[12] M. Di Fabrizio, S. Lupi, A. D'Arco, Virus recognition with Terahertz radiation: drawbacks and potentialities, J. Phys. Photonics 3 (3) (2021) 032001, http://dx.doi.org/10.1088/2515-7647/abfd08.

[13] X. Yang, X. Zhao, K. Yang, Y. Liu, Y. Liu, W. Fu, Y. Luo, Biomedical Applications of Terahertz Spectroscopy and Imaging, Trends Biotechnol. 34 (1) (2016) 810–825, http://dx.doi.org/10.1016/j.tibtech.2016.04.008.

[14] P.U. Jepsen, D.G. Cooke, M. Koch, Terahertz spectroscopy and imaging – Modern techniques and applications, Laser Photonics Rev. 5 (1) (2011) 124–166, http://dx.doi.org/10.1002/lpor.201000011.

[15] A. Paudel, D. Raijada, J. Rantanen, Raman spectroscopy in pharmaceutical product design, Adv. Drug Deliv. Rev. 89 (2015) 3–20, http://dx.doi.org/10.1016/j.addr.2015.04.003.

[16] A. Baran, A. Fiedler, H. Schulz, M. Baranska, In situ Raman and IR spectroscopic analysis of indigo dye, Anal. Methods 2 (2010) 1372–1376, http://dx.doi.org/10.1039/c0ay00311e.

[17] M. Baqué, F. Hanke, U.U. Böttger, T. Leya, R. Moeller, J. de Vera, Protection of cyanobacterial carotenoids' Raman signatures by Martian mineral analogues after high-dose gamma irradiation, J. Raman Spectrosc. 49 (10) (2018) 1617–1627, http://dx.doi.org/10.1002/jrs.5449.

[18] B.C. Smith, How an FTIR works, in: B. Glunn (Ed.), Foundamentals of Fourier Transform Infrared Spectroscopy, second ed., Taylor&Francis, Florida, 2011, pp. 19–53.

[19] L.R. Dartnell, M.C. Storrie-Lombardi, C.W. Mulineaux, A.V. Ruban, G. Wright, A.D. Griffiths, J. Muller, J.M. Ward, Degradation of Cyanobacterial Biosignatures by Ionizing Radiation, Astrobiology 11 (10) (2011) 997–1016, http://dx.doi.org/10.1089/ast.2011.0663.

[20] G.I. Dovbeshko, N.Y. Gridina, E.B. Kruglova, O.P. Pashchuk, FTIR spectroscopy studies of nucleic acid damage, Talanta 53 (1) (2000) 233–246, http://dx.doi.org/10.1016/S0039-9140(00)00462-8.

[21] W. Mihoubi, E. Sahli, A. Gargouri, C. Amiel, FTIR spectroscopy of whole cells for the monitoring of yeast apoptosis mediated by p53 overexpression and its suppression by nigella sativa extracts, PLoS One 12 (7) (2017) e0180680, http://dx.doi.org/10.1371/journal.pone.0180680.

[22] P. Demir, F. Severcan, Monitoring radiation induced alterations in biological systems, from molecules to tissues, through infrared spectroscopy, Appl. Spectrosc. Rev. 51 (10) (2016) 839—863, http://dx.doi.org/10.1080/05704928.2016.1193813.

[23] G. Cakmak, L.M. Miller, F. Zorlu, F. Severcan, Amifostine, a radioprotectant agent, protects rat brain tissue lipids against ionizing radiation induced damage: An FTIR microspectroscopic imaging study, Arch. Biochem. Biophys. 520 (2) (2012) 67–73, http://dx.doi.org/10.1016/j.abb.2012.02.012.

[24] A. Gianoncelli, L. Vaccari, G. Kourousias, D. Cassese, D.E. Bedolla, S. Kenig, P. Storici, M. Lazzarino, M. Kiskinova, Soft X-Ray Microscopy Radiation Damage On Fixed Cells Investigated With Synchrotron Radiation FTIR Microscopy, Sci. Rep. 5 (10250) (2015) http://dx.doi.org/10.1038/srep10250.

[25] A. Filtschew, D. Stranz, C. Hess, Mechanism of NO2 storage in ceria studied using combined in situ Raman/FT-IR spectroscopy, Phys. Chem. Chem. Phys. 15 (2013) 9066–9069, http://dx.doi.org/10.1039/c3cp51441b.

[26] S. Tofani, W. Fuscaldo, Fabry-Perot Cavity Leaky Wave Antennas with Tunable Features for Terahertz Applications, Condens. Matter 5 (11) (2020) http://dx.doi.org/10.3390/condmat5010011.

[27] S.J. Rezvani, D.D. Gioacchino, S. Tofani, A. D'Arco, C. Ligi, S. Lupi, C. Gatti, M.C. Guidi, A. Marcelli, A cryogenic magneto-optical device for long wavelength radiation, Rev. Sci. Instrum. 91 (7) (2020) 075103, http://dx.doi.org/10.1063/5.0011348.

[28] H. Pi, T. Rahman, S.A. Boden, T. Ma, J. Yan, X. Fang, Integrated vortex beam emitter in the THz frequency range: Design and simulation, APL Photonics 5 (7) (2020) 076102–1–8, http://dx.doi.org/10.1063/5.0010546.

[29] A. D'Arco, L. Tomarchio, V. Dolci, P. Di Pietro, A. Perucchi, S. Mou, M. Petrarca, S. Lupi, Broadband Anisotropic Optical Properties of the Terahertz Generator HMQ-TMS Organic Crystal, Condens. Matter 5 (3) (2020) 47, http://dx.doi.org/10.3390/condmat5030047.

[30] M. Jazbinsek, U. Puc, A. Abina, A. Zidansek, Organic Crystals for THz Photonics, Appl. Sci. 9 (5) (2019) 882, http://dx.doi.org/10.3390/app9050882.

[31] H. Guerboukha, K. Nallappan, S. M., Toward real-time terahertz imaging, Adv. Opt. Photonics 10 (4) (2018) 843–938, http://dx.doi.org/10.1364/AOP.10.000843.

[32] E. Castro-Camus, M. Alfaro, Photoconductive devices for terahertz pulsed spectroscopy: A review, Photon. Res. 4 (3) (2016) A36–A42, http://dx.doi.org/10.1364/PRJ.4.000A36.

[33] M. Di Fabrizio, A. D'Arco, S. Mou, L. Palumbo, M. Petrarca, S. Lupi, Performance evaluation of a THz pulsed imaging system: Point Spread Function, Broadband THz Beam Visualization and Image Reconstruction, Appl. Sci. 11 (2) (2021) 562, http://dx.doi.org/10.3390/app11020562.

[34] A. Ren, A. Zahid, D. Fan, X. Yang, M.A. Imran, A. Alomainy, Q.H. Abasi, State-of-the-art in terahertz sensing for food and water security – A comprehensive review, Trend Food Sci. Technol. 85 (2019) 241–251, http://dx.doi.org/10.1016/j.tifs.2019.01.019.

[35] K. Wang, D.W. Sun, H. Pu, Emerging non-destructive terahertz spectroscopic imaging technique: Principle and applications in the agri-food industry, Trend Food Sci. Technol. 67 (2017) 93–105, http://dx.doi.org/10.1016/j.tifs.2017.06.001.

[36] J. Neu, S. Ostresh, K.P. Regan, J.A. Spies, C.A. Schmuttenmaer, Influence of Dye Sensitizers on Charge Dynamics in SnO2 Nanoparticles Probed with THz Spectroscopy, J. Phys. Chem. C 124 (6) (2020) 3482—3488, http://dx.doi.org/10.1021/acs.jpcc.9b11024.

[37] A. D'Arco, M. Di Fabrizio, V. Dolci, M. Petrarca, S. Lupi, THz pulsed imaging in biomedical applications, Condens. Matter 5 (2) (2020) 25, http://dx.doi.org/10.3390/condmat5020025.

[38] J.S. Melinger, Y. Yang, M. Mandehgar, D. Grischkowsky, THz detection of small molecule vapors in the atmospheric transmission windows, Opt. Express 20 (6) (2012) 6788–6807, http://dx.doi.org/10.1364/OE.20.006788.

[39] A. Curcio, A. Marocchino, V. Dolci, S. Lupi, M. Petrarca, Resonant plasma excitation by single-cycle THz pulses, Sci. Rep. 8 (1) (2018) 1052–1059, http://dx.doi.org/10.1038/s41598-017-18312-y.

[40] V. Galstyan, A. D'Arco, M. Di Fabrizio, N. Poli, S. Lupi, E. Comini, Detection of volatile organic compounds: From chemical gas sensors to terahertz spectroscopy, Rev. Anal. Chem. 40 (1) (2021) 33–57, http://dx.doi.org/10.1515/revac-2021-0127.

[41] X. Yang, K. Yang, Y. Luo, W. Fu, Terahertz Spectroscopy for Bacterial Detection: Opportunities and Challenges, Appl. Microbiol. Biotechnol. 100 (12) (2016) 5289–5299, http://dx.doi.org/10.1007/s00253-016-7569-6.

[42] T. Globus, T. Dorofeeva, I. Sizov, B. Gelmont, M. Lvovska, T. Khromova, O. Chertihin, Y. Koryakina, Sub-THz vibrational spectroscopy of bacterial cells and molecular components, Am. J. Biomed. Eng. 2 (4) (2012) 143–154, http://dx.doi.org/10.5923/j.ajbe.20120204.01.

[43] X. Yang, D. Wei, S. Yan, Y. Liu, S. Yu, M. Zhang, Z. Yang, X. Xhu, Q. Huang, H.L.M. Cui, W. Fu, Rapid label-free detection and assessment of bacteria by terahertz time-domain spectroscopy, J. Biophotonics 9 (10) (2016) 1050–1105, http://dx.doi.org/10.1002/jbio.201500270.

[44] J. Jehlička, H.G.M. Edwards, K. Osterrothová, J. Novotná, L. Nedbalová, J. Kopecký, I. Němec, A. Oren, Potential and Limits of Raman Spectroscopy for Carotenoid Detection in Microorganisms: Implications for Astrobiology, Philos. Trans. R. Soc. 372 (2023) (2007) 1–17, http://dx.doi.org/10.1098/rsta.2014.0199.

[45] J. De Gelder, K. De Gussem, P. Vandenabeele, P. Moens, Reference database of Raman spectra of biological molecules, J. Raman Spectrosc. 38 (9) (2007) 1133—1147, http://dx.doi.org/10.1002/jrs.1734.

[46] M. Macernis, J. Sulskus, S. Malickaja, B. Robert, L. Valkunas, Resonance Raman Spectra and Electronic Transitions in Carotenoids: A Density Functional Theory Study, Phys. Chem. A 118 (10) (2014) 1817—1825, http://dx.doi.org/10.1021/jp406449c.

[47] J.H. Crowe, F.A. Hoekstra, L.M. Crowe, Anhydrobiosis, Annu. Rev. Physiol. (54) (1992) 579–599, http://dx.doi.org/10.1146/annurev.ph.54.030192.003051.

[48] C.B. Fox, R.H. Uibel, J.M. Harris, Detecting Phase Transitions in Phosphatidylcholine Vesicles by Raman Microscopy and Self-Modeling Curve Resolution, J. Phys. Chem. B 111 (39) (2007) 11428–11436, http://dx.doi.org/10.1021/jp0735886.

[49] M.J.L. de Lange, M. Bonnb, M. Müller, Direct measurement of phase coexistence in DPPC/cholesterol vesicles using Raman spectroscopy, Chem. Phys. Lipids 146 (2) (2007) 76–84, http://dx.doi.org/10.1016/j.chemphyslip.2006.12.007.

[50] M.J. Balgoon, ATR-IR study of the mechanism of aluminum chloride induced alzheimer's disease; curative and protective effect of lipidium sativum water extract on hippocampus rats brain tissue, J. Pharm. Pharm. Sci. 9 (11) (2015) 786–796, http://dx.doi.org/10.5281/zenodo.1110153.

[51] H.L. Casal, H.H. Mantsch, Polymorphic Phase Behaviour of Phospholipid Membranes Studied by Infrared Spectroscopy, Biochim. Biophys. Acta 779 (1984) 381–401, http://dx.doi.org/10.1016/0304-4157(84)90017-0.

[52] E. Fardelli, M. Lucidi, M. Di Gioacchino, S. Bashiri, L. Persichetti, G. Capecchi, T. Gasperi, A. Sodo, P. Visca, G. Capellini, Bio-physical mechanisms of dehydrating membranes of acinetobacter baumannii linked to drought-resistance, Biochim. Biophys. Acta - Biomembr. 1864 (12) (2022) 184045, http://dx.doi.org/10.1016/j.bbamem.2022.184045.

[53] F. Piccirilli, F. Tardani, A. D'Arco, G. Birarda, L. Vaccari, S. Sennato, S. Casciardi, S. Lupi, Infrared Nanospectroscopy Reveals DNA Structural Modifications upon Immobilization onto Clay Nanotubes, Nanomaterials 11 (5) (2021) 1103, http://dx.doi.org/10.3390/nano11051103.

[54] D.G. Cameron, D.J. Moffatt, A generalized approach to derivative spectroscopy, Appl. Spectrosc. 41 (4) (1987) 539–544, URL https://opg.optica.org/as/abstract.cfm?uri=as-41-4-539.

[55] J. Kong, S. Yu, Fourier transform infrared spectroscopic analysis of protein secondary structures, Acta Biochimica Biophys. Sinica 39 (8) (2007) 549–559, http://dx.doi.org/10.1111/j.1745-7270.2007.00320.x.

[56] H. Yang, S. Yang, J. Kong, A. Dong, S. Yu, Obtaining information about protein secondary structures in aqueous solution using Fourier transform IR spectroscopy, Nat. Protoc. 10 (3) (2015) 382–396, http://dx.doi.org/10.1038/nprot.2015.024.

[57] M. Polsinelli, M. De Felice, A. Galizzi, E. Galli, G. Mastromei, P. Mazza, V. G, Microbiologia, edn, Bollati Boringhieri, Torino, Italy, 1993.

[58] W. Yi, J. Yu, Y. Xu, F. Wang, Q. Yu, H. Sun, L. Xu, Y. Liu, L. Jiang, Broadband terahertz spectroscopy of amino acids, Instrum. Sci. Technol. 45 (5) (2017) 423–439, http://dx.doi.org/10.1080/10739149.2016.1270961.

[59] K. Yamamoto, K. Tominaga, H. Sasakawa, A. Tamura, H. Murakami, H. Ohtake, N. Sarukura, Terahertz time-domain spectroscopy of amino acids and polypeptides, Biophys. J. 89 (2005) L22–L24, http://dx.doi.org/10.1529/biophysj.105.067447.

[60] P. Chamorro-Posada, I. Silva-Castro, J. José Vázquez-Cabo, P. Martín-Ramos, J.M. López-Santos, J. Martín-Gil, A Study of the Far Infrared Spectrum of N-Acetyl-D-Glucosamine Using THz-TDS, FTIR, and Semiempirical Quantum Chemistry Methods, J. Spectroscopy 2016 (2016) 2314–4920, http://dx.doi.org/10.1155/2016/4058478.

[61] W. Wang, H. Li, Y. Zhang, C. Zhang, Correlations Between Terahertz Spectra and Molecular Structures of 20 Standard α-Amino Acids, Acta Phys. Chim. Sin. 25 (10) (2009) 2074—2079, http://dx.doi.org/10.3866/PKU.WHXB20090931.

[62] P.F. Taday, I.V. Bradley, D.D. Arnone, Terahertz pulse spectroscopy of biological Materials: L-Glutamic acid, J. Biol. Phys. 20 (2003) 109–115, http://dx.doi.org/10.1023/A:1024424205309.

[63] J. Tang, B. Yang, B. Llewellyn, R.R. Cutler, R.S. Donnan, Bacillus spores and their relevant chemicals studied by terahertz time domain spectroscopy, Chem. Phys. Lett. 592 (2014) 302–306, http://dx.doi.org/10.1016/j.cplett.2013.12.061.

[64] T. Mancini, R. Mosetti, A. Marcelli, M. Petrarca, S. Lupi, A. D'Arco, Terahertz spectroscopic analysis in protein dynamics: Current status, Radiation 2 (1) (2022) 100–123, http://dx.doi.org/10.3390/radiation2010008.

[65] C. Song, W. Fan, L. Ding, X. Chen, Z. Chen, K. Wang, Terahertz and infrared characteristic absorption spectra of aqueous glucose and fructose solutions, Sci. Rep. (8) (2018) 8964, http://dx.doi.org/10.1038/s41598-018-27310-7.

[66] Y. Bian, X. Zhang, Z. Zhu, B. Yang, Vibrational modes optimization and terahertz time-domain spectroscopy of L-lysine and L-lysine hydrate, Sci. Rep. 1232 (2021) 129952, http://dx.doi.org/10.1016/j.molstruc.2021.129952.

[67] M. Yamaguchi, F. Miyamaru, K. Yamamoto, M. Tani, M. Hangyo, Terahertz absorption spectra of L-, D-, and DL-alanine and their application to determination of enantiometric composition, Appl. Phys. Lett. 86 (2005) 053903, http://dx.doi.org/10.1063/1.1857080.

[68] Z. Zheng, W. Fan, H. Li, T. J., Terahertz spectral investigation of anhydrous and monohydrated glucose using terahertz spectroscopy and solid-state theory, J. Mol. Spectrosc. 296 (2014) 9–13, http://dx.doi.org/10.1016/j.jms.2013.12.002.

[69] A. Conter, D. Dupouy, H. Planel, Influence of growth phase on radiation stimulation of proliferation in *Synechococcus* lividus in culture, Radiat. Res. 99 (1984) 651—658, http://dx.doi.org/10.2307/3576338.

[70] M.J. Kraus, Resistance of blue-green algae to 60Co gamma radiation, Radiat. Bot. 9 (6) (1969) 481–489, http://dx.doi.org/10.1016/S0033-7560(69)80054-2.

[71] A. Conter, D. Dupouy, H. Planel, Light modulation of radiosensitivity of Synechococcus lividus to very low doses of ionizing radiation, Environ. Exp. Bot. 24 (3) (1984) 229–237, http://dx.doi.org/10.1016/0098-8472(84)90003-0.

[72] W. Leyko, G. Bartosz, Membrane effects of ionizing radiation and hyperthermia, Int. J. Radiat. Biol. 49 (2000) 743—770.

[73] M. Scheller, C. Jansen, M. Koch, Applications of effective medium theories in the terahertz regime, in: K.Y. Kim (Ed.), Recent Optical and Photonic Technologies, InTech, 2010.

[74] J.M. Monteiro, P.B. Fernandes, F. Vaz, A.R. Pereira, A.C. Tavares, M.T. Ferreira, P.M. Pereira, H. Veiga, E. Kuru, M.S. VanNieuwenhze, Y.V. Brun, S.R. Filipe, M.G. Pinho, Resistance of blue-green algae to 60Co gamma radiation, Nature Commun. 6 (1) (2015) 8055, http://dx.doi.org/10.1038/ncomms9055.

[75] A.C. Cockell, D. Billi, E.I. Friedmann, C. Panitz, Effects of a Simulated Martian UV Flux on the Cyanobacterium, *Chroococcidiopsis* sp. 029, Astrobiology 5 (2) (2005) 127–140, http://dx.doi.org/10.1089/ast.2005.5.127.

[76] E.J. Hall, A.J. Giaccia, Radiobiology for the Radiologist, seventh ed., Lippincott Williams & Wilkins, Pennsylvania, 2012, pp. 9–11, 104–114.

[77] M. Baqué, C. Verseux, U. Böttger, E. Rabbow, J.P. de Vera, D. Billi, Preservation of biomarkers from cyanobacteria mixed with mars like regolith under simulated martian atmosphere and UV flux, Orig. Life Evol. Biosph. 46 (2-3) (2016) 289–310, http://dx.doi.org/10.1007/s11084-015-9467-9.

[78] H.G.M. Edwards, I.B. Hutchingson, R. Ingley, N.R. Waltham, S. Beardsley, S. Dowson, S. Woodward, The search for signatures of early life on Mars: Raman spectroscopy and the Exomars mission, Europe, Spectroscopy 23 (1) (2011) 6–15.

[79] B. Yu, A. Alimova, A. Katz, R.R. Alfano, Terahertz and Gigahertz Electronics and Photonics IV, SPIE, Digital Library, 2005, pp. 20–23, 5727.

[80] S.K. Bhardwaj, N. Bhardwaj, V. Kumar, D. Bhatt, A. Azzouz, J. Bhaumik, K.H. Kim, D. A, Recent progress in nanomaterial-based sensing of airborne viral and bacterial pathogens, Environ. Int. 146 (2021) 106183, http://dx.doi.org/10.1016/j.envint.2020.106183.

[81] L. Manti, A. D'Arco, Cooperative biological effects between ionizing radiation and other physical and chemical agents, Mutat. Res. 704 (1–3) (2010) 115–122, http://dx.doi.org/10.1016/j.mrrev.2010.03.005.

[82] C. Fagliarone, A. Napoli, S. Chiavarini, M. Baqué, J.-P. de Vera, D. Billi, Biomarker preservation and survivability under extreme dryness and Mars-like UV flux of a desert cyanobacterium capable of trehalose and sucrose accumulation, Front. Astron. Space Sci. 7 (2020) 31, http://dx.doi.org/10.3389/fspas.2020.00031.

[83] M. Di Gioacchino, F. Bruni, M.A. Ricci, Protection against Dehydration: A Neutron Diffraction Study on Aqueous Solutions of a Model Peptide and Trehalose, J. Phys. Chem. B 122 (45) (2018) 10291–10295, http://dx.doi.org/10.1021/acs.jpcb.8b08046.

[84] M. Di Gioacchino, M.A. Ricci, S. Imberti, N. Holzmann, B. F, Hydration and aggregation of a simple amino acid: The case of glycine, J. Mol. Liq. 301 (2020) 112407, http://dx.doi.org/10.1016/j.molliq.2019.112407.